Mismatched Complementary-on-Receive Filtering (MiCRFt) for MIMO Radar

Matthew B. Heintzelman, Christian C. Jones, Patrick M. McCormick, Shannon D. Blunt
Radar Systems Lab (RSL), University of Kansas, Lawrence KS

***Abstract*–While the suppression of range sidelobes has received considerable attention, with a variety of solutions now possible, the mitigation of cross-correlation sidelobes for multistatic/MIMO scenarios remains a difficult problem. Here, leveraging the recent MiCRFt method that was experimentally shown to achieve complementary receive cancellation, a multi-emitter extension is posed that provides the degrees-of-freedom necessary to reduce both auto- and cross-correlation sidelobes. The ensuing MIMO MiCRFt formulation is experimentally demonstrated using simulated, loopback, and open-air measurements obtained using random FM (RFM) nonrepeating waveforms.**

Keywords–MIMO radar, multistatic radar, mismatched filtering, inverse filtering, least squares, waveform diversity, noise waveforms

I. INTRODUCTION

The combination of high radar transmit power (up to ~10^6 W) and low receive power (down to ~10^{-18} W) can introduce electromagnetic fratricide problems [1] between different radars occupying the same spectrum if careful management between systems is not performed (i.e. not pointing a high-power transmit beam directly at a sensitive receiver). However, even when fratricide can be avoided, such as in the case of colocated multiple-input multiple-output (MIMO) operation, there still remains the issue of sufficient waveform separability.

Because scattering is a continuum (i.e. not discrete points) over range and spatial angle, the notion of so-called "orthogonal" radar waveforms is not physically meaningful in the context of shared-spectrum operation (notwithstanding the trivial case of time-division multiplexing that expands the resource management timeline and reduces the unambiguous range interval) [2]. Consequently, quasi-orthogonal (QuO) waveforms having low cross-correlation are of great interest. Of course, a given waveform has finite degrees-of-freedom (DoFs) according to its time-bandwidth product (*TB*). As a dimensionality metric, *TB* dictates both the autocorrelation sidelobes achievable by receiver matched filtering and the cross-correlation sidelobes that the same matched filter would encounter when applied to a different waveform [3]. This cross-correlation fundamentally limits the performance of previously theorized code division multiple access transmit schemes for MIMO radar [4, 5, 6].

It has been shown [7] that the use of nonrepeating (pulsed) waveforms introduces an "aggregate *TB*" attribute that multiplicatively expands waveform dimensionality, thereby likewise reducing the achievable autocorrelation and cross-correlation sidelobes by the same factor. For example, the separability of two arbitrary frequency modulated (FM) waveforms having $TB = 1000$ is, on average, on the order of $-10\log_{10}(TB) = -30$ dB. By extension, two independent streams of $M = 10^4$ nonrepeating waveform sets with the same *TB* would yield separability on the order of $-10\log_{10}(M \bullet TB) = -70$ dB. However, if even higher receiver dynamic range is required, or if *TB* and/or *M* are more modest for a given application, transmit dimensionality alone may not suffice.

To contend with inadequate waveform separability the multistatic adaptive pulse compression (MAPC) algorithm was developed [8] and later experimentally demonstrated [9] as a means to iteratively separate the received scattering induced by different radar waveforms that are coincident in time and spectral occupancy. Being adaptive, this approach can suppress cross (and auto) correlation sidelobes down to the noise floor, suggesting it should be applied as late as possible in the receive processing chain to make best use of coherent gain. However, doing so may complicate other processing stages, such as necessitating enhanced range-walk compensation [9].

Here we instead consider an expansion of the well-known least squares (LS) mismatched filter (MMF) [10, 11] to provide additional separability between dissimilar, spectrally-coincident emissions. Noting that the LS-MMF is defined in the context of a single emitter (i.e. no cross-correlation), it uses the available DoFs from waveform *TB* to suppress "self" correlation sidelobes (the MMF no longer truly yields an autocorrelation). Care must be taken to limit the amount of mismatch loss, which can be particularly severe if super-resolution or range-straddling occurs; hence phase-continuous waveforms and preservation of the nominal matched filter resolution are preferred [11, 12, 13].

On its face, attempting to directly extend the LS-MMF to address both cross-correlation and self-correlation sidelobes is hindered by insufficient DoFs. Thus, we shall expand the available DoFs by modifying the mismatched complementary-on-receive filtering (MiCRFt) formulation [14, 15], which jointly solves for LS-MMFs for subsets of contiguous waveforms so that the resulting mismatch filtered responses can be combined before Doppler processing to suppress range sidelobes. When used in conjunction with nonrepeating waveforms, MiCRFt has been demonstrated experimentally and in simulation to greatly reduce the range sidelobe modulation (RSM) that arises from time-varying self-correlation sidelobes over the coherent processing interval (CPI). The version here, denoted as MIMO-MiCRFt, extends to multiple concurrent emissions, and is likewise demonstrated experimentally and in simulation to suppress both self-correlation RSM and similar cross-correlation modulation (CCM). It is also shown that the latter effect is not adequately addressed by standard single-waveform filtering methods.

This work was supported by the Office of Naval Research under Contract #N00014-23-C-1053. DISTRIBUTION STATEMENT A. Approved for Public Release.

II. Multi-Emitter Single-Pulse LS-MMF Design

The standard LS-MMF pulse compression problem is formulated as follows: construct the L-length FIR filter $\mathbf{w}$ such that the output matches some desired response. The LS-MMF filter is then realized by solving

$$\min_{\mathbf{w}} \|\mathbf{S}\mathbf{w} - \mathbf{d}\|_2^2 , \tag{1}$$

where $\mathbf{S}$ is an $(L+N-1)\times L$ convolution matrix constructed from delay-shifted versions of N-length vector $\mathbf{s}$ obtained by discretizing waveform $s(t)$ to capture sufficient spectral roll-off, and $\mathbf{d}$ is the desired response having length $(L+N-1)$. The exact form of $\mathbf{d}$ is somewhat arbitrary, though it was shown [11] that choosing the mainlobe of the matched filter, with zeros elsewhere, provides a good tradeoff between SNR loss and sidelobe level. Alternatively, [16] sets the desired response according to the waveform spectral design template. Both approaches can preserve the matched filter nominal resolution and thereby mitigate the severe loss that tends to accompany super-resolution.

It should be noted that (1) is a convex problem. As such, the regularized solution for a single waveform is

$$\mathbf{w}_{\mathrm{LS}} = \left(\mathbf{S}^H\mathbf{S} + \mu\mathbf{I}\right)^{-1}\mathbf{S}^H\mathbf{d} \tag{2}$$

for LS-optimal filter $\mathbf{w}_{\mathrm{LS}}$ and diagonal loading factor μ.

We could also generalize (1) to account for the superimposed effects of K distinct emissions. Define $\mathbf{z}_{ki}$ as the convolution between the waveform emitted by transmitter k (in discretized form) and receive filter i (for ith transmit waveform) as

$$\mathbf{z}_{ki} = \mathbf{S}_k\mathbf{w}_i . \tag{3}$$

The multi-emitter optimization problem for the ith receive filter is therefore

$$\min_{\mathbf{w}_i} \sum_{k=0}^{K-1} J_k(\mathbf{w}_i) \tag{4}$$

where

$$J_k(\mathbf{w}_i) = \begin{cases} \|\mathbf{S}_{\boldsymbol{k}}\mathbf{w}_i - \mathbf{d}_i\|_2^2 & , \text{ for } i = k \\ \|\mathbf{S}_{\boldsymbol{k}}\mathbf{w}_i - \mathbf{0}\|_2^2 & , \text{ for } i \neq k \end{cases} \tag{5}$$

for $i,k \in \{0,1,\ldots,K\}$, which states that the desired pulse-compressed MIMO response is $\mathbf{z}_{ki} = \mathbf{d}_i\,\delta[k-i]$ for $\delta[k]$ the discrete delta function. Assuming the design statements in (5) all possess equal importance; we can collect them into a single design statement by adopting block matrix notation as

$$\min_{\mathbf{w}_i} \left\|\overline{\mathbf{S}}\mathbf{w}_i - \overline{\mathbf{d}}_i\right\|_2^2, \tag{6}$$

in which $\overline{\mathbf{S}} = \left[\mathbf{S}_1^T\ \mathbf{S}_2^T\ \ldots\ \mathbf{S}_K^T\right]^T$ and $\overline{\mathbf{d}}_i = \mathbf{e}_i \otimes \mathbf{d}_i$, for elementary vector $\mathbf{e}_i$ and $\otimes$ the Kronecker product. Therefore, the objective in optimizing $\mathbf{w}_i$ is to yield desired response $\mathbf{d}_i$ when applied to the ith transmit waveform while minimizing the response to the remaining K–1 waveforms. The ensuing solution to (6) is

$$\mathbf{w}_{\mathrm{ME},i} = \left(\overline{\mathbf{S}}^H\overline{\mathbf{S}} + \mu\mathbf{I}\right)^{-1}\overline{\mathbf{S}}^H\overline{\mathbf{d}}_i , \tag{7}$$

where $\mathbf{w}_{\mathrm{ME},i}$ is the regularized multi-emitter (ME) least squares filter. As shown later, (7) provides marginal improvement over the LS-MMF from (2) since the limitation of both is insufficient DoFs to address cross-correlation, which is addressed next.

III. Multi-Emitter Multi-Pulse LS-MMF Design

The goal of complementary design (be that for waveforms [17, 18] or filters [14]) is to increase DoFs as a means of improving sidelobe suppression. Here, pulse compression filters are designed such that the superposition of their responses combine coherently to provide cancellation of both self- and cross-correlation sidelobes.

To avoid confusion with the term "pre-summing", which has been used in the context of slow-time receive combining (of repeated waveforms) both before and after pulse compression, we use "post-summing" for the latter. Consequently, post-summing the responses from P consecutive pulses modulated with unique waveforms (having the same spectral support) is now equated with the desired response for the ith receiver. Of course, post-summing results in a reduction in the observable Doppler space by a factor of P and incurs some coherence loss for fast movers that exhibit a phase ramp across slow-time (ignored during post-summing). As an extension of (5), we seek to determine a set of P LS-MMFs such that

$$J_k\left(\mathbf{w}_{i1},\mathbf{w}_{i2},..,\mathbf{w}_{ip}\right) = \begin{cases} \left\|\sum_{p=1}^{P}\mathbf{S}_{kp}\mathbf{w}_{ip} - \overline{\mathbf{d}}_i\right\|_2^2 & , \text{ for } i = k \\ \left\|\sum_{p=1}^{P}\mathbf{S}_{kp}\mathbf{w}_{ip} - \mathbf{0}\right\|_2^2 & , \text{ for } i \neq k \end{cases} . \tag{8}$$

Like (6), we can rewrite the multi-emitter optimization problem (4), using the complementary cost functions in (8), in block form as

$$\min_{\overline{\mathbf{w}}_i} \left\|\overline{\overline{\mathbf{S}}}\,\overline{\mathbf{w}}_i - \overline{\mathbf{d}}_i\right\|_2^2 , \tag{9}$$

where matrix $\overline{\overline{\mathbf{S}}} = [\overline{\mathbf{S}}_1\ \overline{\mathbf{S}}_2\ \ldots\ \overline{\mathbf{S}}_P]$ is comprised of P convolution block matrices, which for the pth pulse takes the form $\overline{\mathbf{S}}_p = [\mathbf{S}_{1p}^T\ \mathbf{S}_{2p}^T\ \ldots\ \mathbf{S}_{Kp}^T]^T$ for K concurrently emitted waveforms, and the associated concatenated filterbank $\overline{\mathbf{w}}_i = [\mathbf{w}_{i1}^T\ \mathbf{w}_{i2}^T\ \ldots\ \mathbf{w}_{ip}^T]^T$. We can further expand to encompass all K pulse-compression filters (agnostic to the particular receiver) as

$$\min_{\overline{\mathbf{W}}} \left\|\overline{\overline{\mathbf{S}}}\,\overline{\mathbf{W}} - \overline{\mathbf{D}}\right\|_2^2 , \tag{10}$$

where $\overline{\mathbf{W}}$ is the block filterbank matrix whose kth column is comprised of the P LS-MMFs corresponding to transmitter k, and $\overline{\mathbf{D}}$ is a matrix whose kth column is the desired response for the kth emitter. The MIMO-MiCRFt (MM) solution is therefore

$$\overline{\mathbf{W}}_{\mathrm{MM}} = \left(\overline{\overline{\mathbf{S}}}^H\overline{\overline{\mathbf{S}}} + \mu\mathbf{I}\right)^{-1}\overline{\overline{\mathbf{S}}}^H\overline{\mathbf{D}} . \tag{11}$$

For convenience, the matrices $\overline{\overline{\mathbf{S}}}$, $\overline{\mathbf{W}}$, and $\overline{\mathbf{D}}$ are constructed as

$$\overline{\overline{\mathbf{S}}} = \begin{bmatrix} \mathbf{S}_{11} & \mathbf{S}_{12} & \cdots & \mathbf{S}_{1P} \\ \mathbf{S}_{21} & \mathbf{S}_{21} & \cdots & \mathbf{S}_{2P} \\ \vdots & \vdots & \ddots & \vdots \\ \mathbf{S}_{K1} & \mathbf{S}_{K2} & \cdots & \mathbf{S}_{KP} \end{bmatrix} \in \mathbb{C}^{(L+N-1)K\times LP}, \tag{12}$$

$$\overline{\mathbf{W}} = \begin{bmatrix} \mathbf{w}_{11} & \mathbf{w}_{12} & \cdots & \mathbf{w}_{1K} \\ \mathbf{w}_{21} & \mathbf{w}_{22} & \cdots & \mathbf{w}_{2K} \\ \vdots & \vdots & \ddots & \vdots \\ \mathbf{w}_{P1} & \mathbf{w}_{P2} & \cdots & \mathbf{w}_{PK} \end{bmatrix} \in \mathbb{C}^{LP \times K}, \tag{13}$$

$$\overline{\mathbf{D}} = \begin{bmatrix} \mathbf{d}_1 & \mathbf{0} & \cdots & \mathbf{0} \\ \mathbf{0} & \mathbf{d}_2 & \cdots & \mathbf{0} \\ \vdots & \vdots & \ddots & \vdots \\ \mathbf{0} & \mathbf{0} & \cdots & \mathbf{d}_K \end{bmatrix} \in \mathbb{C}^{(L+N-1)K \times K}. \tag{14}$$

IV. Spectral Considerations

When the interfering waveforms occupy similar spectral footprints, the formulation in (7) does not provide the necessary DoFs to suppress cross-responses without incurring large SNR loss in the self-response. To provide a peak in the self-response, the associated MMF must provide gain in the passband of the corresponding waveform. If interfering waveforms occupy this same band, cross-correlation sidelobe suppression is limited.

Consider the dual-transmitter case depicted in Figs. 1-4 where MMFs are formed according to (7) and (11) and are compared to the matched filter. The two emitters have completely overlapped passbands, resulting in worst-case interference. Here, two unique sets of 500 random FM (RFM) waveforms were generated via the pseudo-random optimized (PRO-FM) approach [12], each having $TB = 64$. The per-waveform separability is therefore $-10\log_{10}(TB) = -18$ dB. The waveform design spectral template is a super-Gaussian function with shape parameter $n = 8$ [19]. Per [16], each MMF desired response is based on the inverse FFT (IFFT) of the RMS combination of the obtained waveform spectra, albeit with sidelobes set to zero (i.e. including only the mainlobe). The diagonal loading factor μ is set to $(TB)^{-4}$, or −72 dB.

Fig. 1 provides a frequency-domain view of the two single-pulse MIMO LS-MMFs from (7), where $S_1(f)$ and $S_2(f)$ are the spectra of the two concurrent waveforms, $W_1(f)$ is the MMF spectra for the former, and $Z_{11}(f)$ and $Z_{12}(f)$ are the ensuing self-correlation and cross-correlation when $W_1(f)$ is applied to each waveform. Since the two emitters have identical spectral occupancy, the MMF is unable to meaningfully reduce cross-correlation interference since the given DoFs are used to suppress self-correlation sidelobes. Fig. 2 in turn illustrates the time-domain view, where the MMF yields 5.2 dB of additional self-correlation sidelobe suppression in $z_{11}(\tau)$, for τ the lag index, at a cost of 3.4 dB of mismatch loss. The 4.4 dB cross-correlation suppression in $z_{12}(\tau)$ is likewise modest. The cross-correlation of −24 dB has an extra −6 dB due to post-summing by 4 to facilitate direct comparison with the following case.

Now consider the case in which $P = 4$ pulses having distinct waveforms are used in this two-emitter context to construct a set of 4×2 MMFs using MIMO-MiCRFt according to (11), the pulse compressed responses of which are post-summed as described in Sect. III. Figs. 3 and 4 show the ensuing frequency- and time-domain results, where $Z_{11}(f)$ appears similar to Fig. 1 while $Z_{12}(f)$ is now greatly attenuated. Per Fig. 4, both the self-correlation sidelobes of $z_{11}(\tau)$ and the cross-correlation interference of $z_{12}(\tau)$ are suppressed by nearly 150 dB. However, the price for this cancellation is 5.1 dB of loss, which is due to a low regularization setting. In subsequent sections, regularization is set to a higher value, thereby admitting higher sidelobes in exchange for much less mismatch loss.

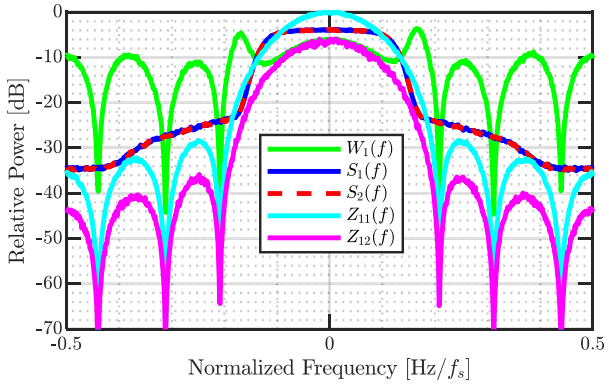

Fig 1: Power spectra for non-complementary LS-MMFs via (7)

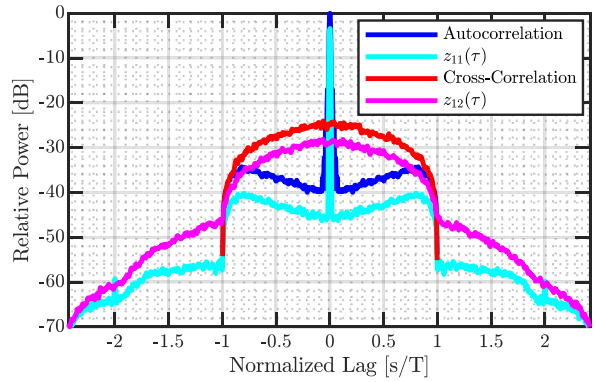

Fig 2: Filter response for non-complementary LS-MMFs via (7)

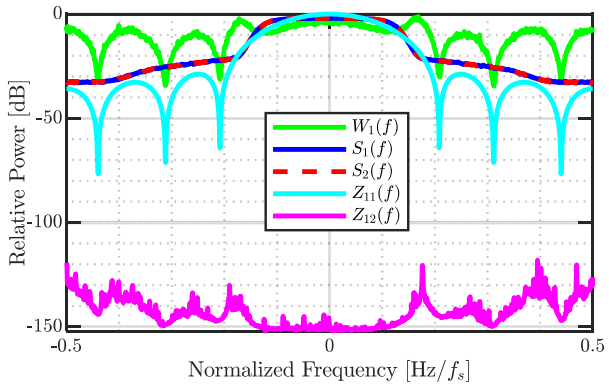

Fig 3: Power spectra for complementary ($P = 4$) MIMO MiCRFt via (11)

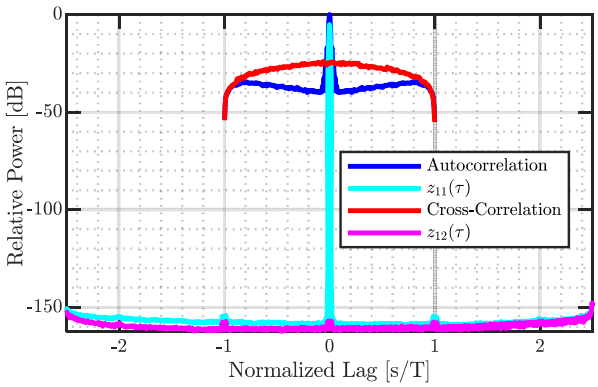

Fig 4: Filter response for complementary ($P = 4$) MIMO MiCRFt via (11)

V. MMF FOR MIMO RADAR (LOOPBACK RESULTS)

Now consider a comparison between four possible candidate pulse compression filters constructed for a dual transmitter arrangement. The candidate filters are the matched filter, standard LS-MMFs (2), MIMO LS-MMFs (7), and the MIMO MiCRFt filterbank (11) for $P = 4$. To provide a fair comparison in terms of dimensionality, the first three cases have their filter outputs post-summed by four as well. For the three LS-derived MMFs, the regularization factor was tuned for a much lower mismatch loss than in Sect. IV (detailed below).

To provide further realism, the super-Gaussian PRO-FM waveforms from Sect. IV were captured in a loopback hardware configuration. A consequence of the spectral containment from super-Gaussian shaping is the appearance of near-in shoulder lobes around the pulse compression mainlobe. For this set of waveforms, the RMS peak value for the shoulder lobes is –17.0 dB (matched filter), which modestly decreases to –17.8 dB, –17.4 dB, and –21.2 dB for LS-MMF, MIMO LS-MMF, and MIMO MiCRFt, respectively. As discussed in [16], these shoulder lobes are persistent attributes that do not experience incoherent averaging suppression like other RFM sidelobes when slow-time processing is performed. However, their close mainlobe proximity makes them effectively indistinguishable from the modest broadening encountered when tapering standard LFM/NLFM waveforms. Therefore, Table 1 excludes these shoulder lobes from the sidelobe metrics.

Fig. 5 depicts the post-summed response of standard LS-MMF from (2) compared with a corresponding matched filter output. While the sidelobe floor of the MMF self-response $z_{11}(\tau)$ is suppressed by roughly 30 dB, the MMF cross-response $z_{12}(\tau)$ is hardly affected (decreasing by 0.8 dB relative to the cross-correlation). With autocorrelation sidelobes already low (typical for PRO-FM), the benefit of this approach is minimal, as illustrated experimentally in the next section.

Fig. 6 shows the MIMO LS-MMF from (7), which seeks to suppress both self- and cross-response sidelobes on a per-pulse basis. Relative to the autocorrelation, $z_{11}(\tau)$ is now slightly raised (by 1.5 dB), but $z_{12}(\tau)$ is reduced by 4 dB, a modest net improvement.

Finally, MIMO MiCRFt via (11) is depicted in Fig. 7. Here both the self-response $z_{11}(\tau)$ and cross-response $z_{12}(\tau)$ are attenuated. Comparing with Fig. 5, we note that $z_{11}(\tau)$ has not quite decreased to the level achieved by standard LS-MMF. Rather, MiCRFt uses the additional DoFs to balance the suppression of both self- and cross-responses.

It is also useful to consider a collective sidelobe floor comprised of both self- and cross-responses for each approach, thereby depicting the limiting behavior. For each filter type, Fig. 8 plots the ensuing sum of self- and cross-responses, where we observe that the matched filters, standard LS-MMFs, and MIMO LS-MMFs all yield quite similar peak sidelobe levels, with the latter the lowest by about 5 dB. In contrast, MIMO MiCRFt provides an additional 20 dB in collective sidelobe suppression. Moreover, mismatch loss is 0.9, 1.55, and 1.54 dB for LS-MMF, MIMO LS-MMF, and MIMO MiCRFt, respectively, indicating that relatively low loss can be achieved.

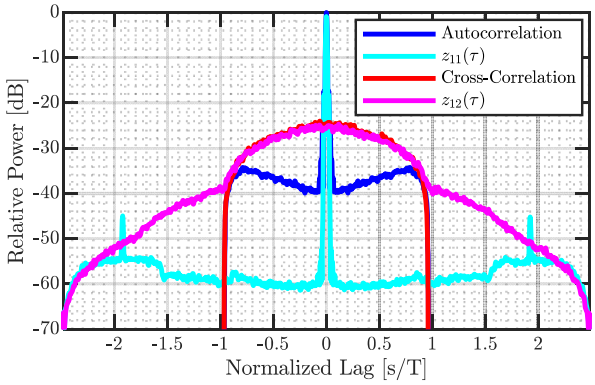

Fig 5: Matched filtering versus LS-MMF from (2) for $P = 4$

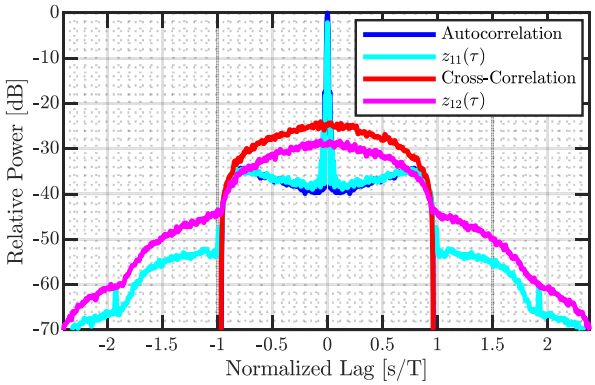

Fig 6: Matched filtering versus MIMO LS-MMF from (7) for $P = 4$

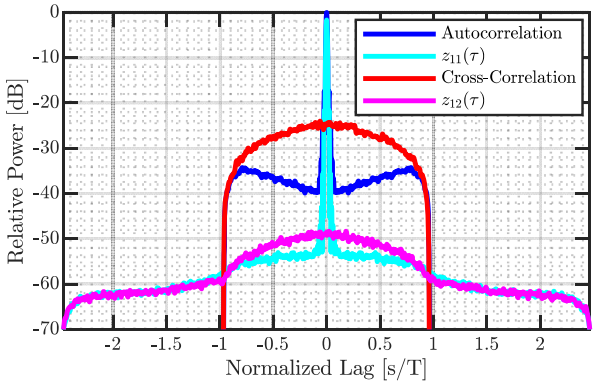

Fig 7: Matched filtering versus MIMO MiCRFt from (11) for $P = 4$

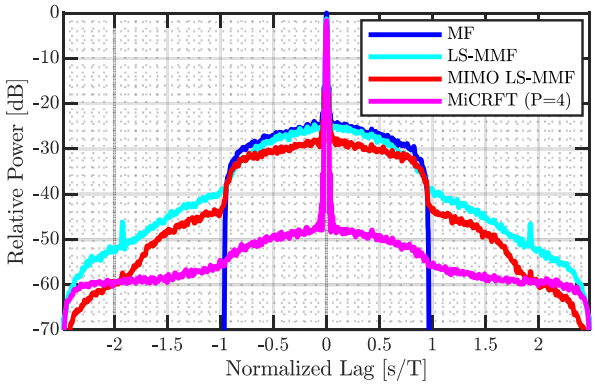

Fig 8: Comparison of collective self- and cross-responses

A quantitative comparison is shown in Table 1 using a variety of performance metrics that are root-mean-square (RMS) combined over the 125 independent responses obtained

for each filter type when the 500 unique loopback waveforms are post-summed in sets of 4. Well-known metrics of peak sidelobe level (PSL), integrated sidelobe level (ISL), and mismatch loss (MML) [3] are shown along with metrics that capture cross-response.

One of these is the peak cross-response level (PCRL) that evaluates the maximum cross-response between a given waveform and filter when both are normalized to have unity Euclidean length. For convolution matrix $\mathbf{S}_k$ formed from discretized waveform $\mathbf{s}_k$ and arbitrary pulse compression filter $\mathbf{w}_i$ (and for $i \neq k$), this metric can be posed as

$$\mathrm{PCRL}_{ki} = \max \left\{ \frac{(\mathbf{S}_k \mathbf{w}_i) \odot (\mathbf{S}_k \mathbf{w}_i)^*}{\|\mathbf{s}_k\|_2^2 \|\mathbf{w}_i\|_2^2} \right\} \text{ for } i \neq k. \quad (15)$$

With (15) a cross-response analog to PSL, we can likewise define an integrated cross-response level (ICRL) akin to ISL as

$$\mathrm{ICRL}_{ki} = \frac{(\mathbf{S}_k \mathbf{w}_i)^H (\mathbf{S}_k \mathbf{w}_i)}{\|\mathbf{s}_k\|_2^2 \|\mathbf{w}_i\|_2^2} \text{ for } i \neq k, \quad (16)$$

which yields the total normalized energy in the filter output.

The pairwise waveform/filter metrics in (15) and (16) can then be extended over the full set of K emitters (ignoring relative received power scaling). Thus, a peak total-interference level (PTIL) extension of (15) quantifies the maximum correlation-induced interference for a set of K independent transmit waveform convolution matrices $\{\mathbf{S}_1, \mathbf{S}_2, \ldots, \mathbf{S}_K\}$ via

$$\mathrm{PTIL}_i = \max \left\{ \left| \frac{\tilde{\mathbf{S}}_i \mathbf{w}_i}{\|\mathbf{s}_i\|_2^2 \|\mathbf{w}_i\|_2^2} + \sum_{\substack{k=1 \\ k \neq i}}^{K} \frac{\mathbf{S}_k \mathbf{w}_i}{\|\mathbf{s}_k\|_2^2 \|\mathbf{w}_i\|_2^2} \right|^2 \right\}, \quad (17)$$

where $\tilde{\mathbf{S}}_i$ is the ith waveform convolution matrix in which the middle $2\lceil f_s/B \rceil - 1$ rows (corresponding to mainlobe samples) are zeroed-out based on oversampling ratio of f_s/B. Similarly, an integrated total interference level (ITIL) extension of (16) provides the total normalized sidelobe energy as

$$\mathrm{ITIL}_i = \frac{\left(\tilde{\mathbf{S}}_i \mathbf{w}_i\right)^H (\tilde{\mathbf{S}}_i \mathbf{w}_i)}{\|\mathbf{s}_i\|_2^2 \|\mathbf{w}_i\|_2^2} + \sum_{\substack{k=1 \\ k \neq i}}^{K} \frac{(\mathbf{S}_k \mathbf{w}_i)^H (\mathbf{S}_k \mathbf{w}_i)}{\|\mathbf{s}_k\|_2^2 \|\mathbf{w}_i\|_2^2}. \quad (18)$$

These metrics are tabulated below for the given set of MMF methods and waveforms, along with mismatch loss (MML). For metrics (15)-(18) that capture the collective sidelobe response it is clear that MIMO-MiCRFt yields superior performance.

Table 1: Pulse Compression Performance Metrics (dB)

	Matched Filter	LS-MMF (2)	MIMO LS-MMF (7)	MIMO-MiCRFT for $P = 4$ (11)
PSL	−34.3	−45.7	−32.4	−53.0
ISL	−16.8	−34.3	−13.9	−33.5
PCRL	−24.0	−24.7	−28.3	−51.1
ICRL	−0.4	−0.8	−4.3	−26.2
PTIL	−24.2	−23.3	−25.9	−48.3
ITIL	−7.4	−16.8	−7.6	−29.6
MML	0	0.90	1.55	1.54

VI. MMF for MIMO Radar (Open-Air Results)

We now use open-air measurements to compare these MMF methods. Here, $K = 2$ collocated emitters transmit the same two sets of 500 unique PRO-FM waveforms assessed in Sects. IV and V, parameterized by a pulsewidth of T=1.28 μs and a 6-dB bandwidth of B = 50 MHz, so $TB = 64$. Each waveform was digitally upconverted to a center frequency of 3.40 GHz and produced by a 2-channel arbitrary waveform generator (AWG). Receive capture was performed by a real-time spectrum analyzer operating at 400 Megasamples/second. The loopback-captured waveforms from Sect. V were used to instantiate the receive filters, again using $P = 4$ post-summing.

The range-Doppler response obtained by matched filtering for emitter $k = 1$ is depicted in Fig. 9, which illustrates the difficulty caused by the superposition of RSM (a self-correlation effect) and cross-correlation sidelobes. As expected from Sect. V, Fig. 10 likewise shows that standard LS-MMFs (each based on a single waveform) provide little additional benefit in this context, yielding 0.9 dB in sidelobe suppression.

When the multi-emitter scenario is addressed on a single-pulse basis for MMF design, per (7), the range-Doppler response in Fig. 11 is realized, with the sidelobe floor reduced by 2.7 dB relative to the matched filter case. In other words, while a MIMO extension to the LS-MMF framework does provide some benefit, there are simply insufficient DoFs to make a meaningful difference. In Fig. 11 it is not yet clear exactly where the movers are located.

The most significant improvement (12.7 dB) is obtained by MIMO MiCRFt in Fig. 12 due to the additional DoFs afforded by complementary combining. Indeed, the full benefit is not even observed in these results because the self-/cross-correlation sidelobes have been pushed below the noise floor, allowing the actual movers to be easily identified.

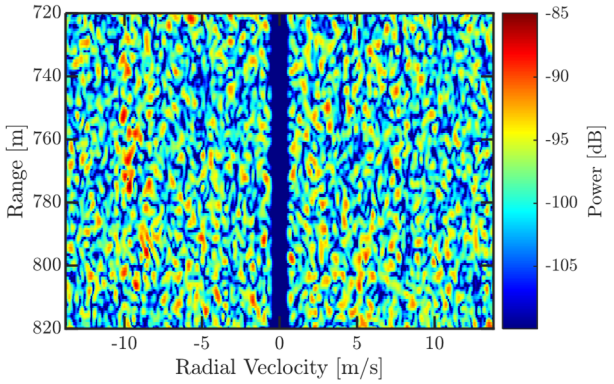

Fig 9: Open-air range-Doppler response for 2 emitters: matched filtering

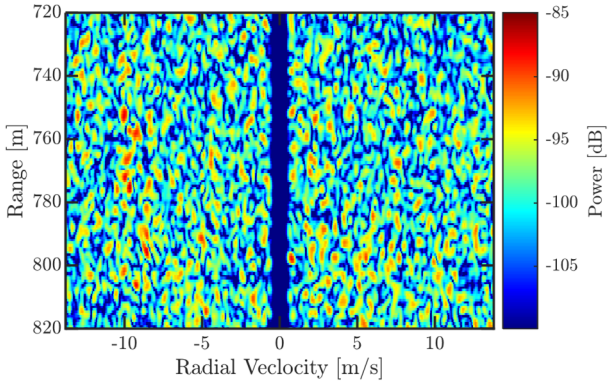

Fig 10: Open-air range-Doppler response for 2 emitters: LS-MMF (2)

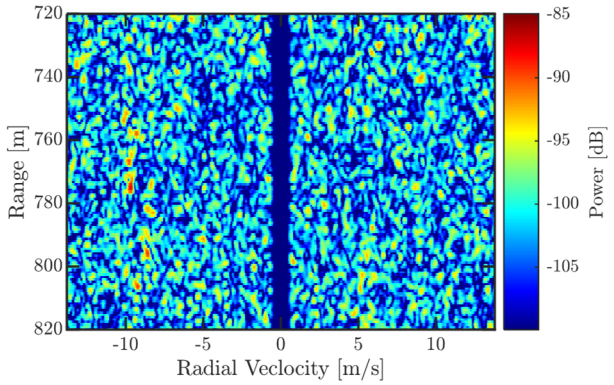

Fig 11: Open-air range-Doppler response for 2 emitters: MIMO LS-MMF (7)

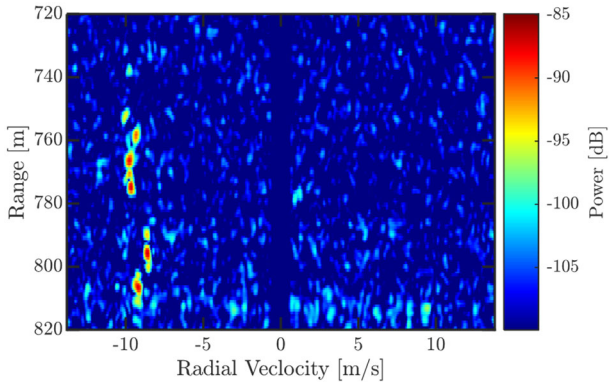

Fig 12: Open-air range-Doppler response for 2 emitters: MIMO MiCRFt (11)

As a final comparison to characterize the improvement in contrast between movers and sidelobe interference, the histograms in Fig. 13 were formed from the samples (in dB) for each of the range-Doppler responses. Comparing the peaks of each histogram (approximating the mode of each underlying distribution) shows the progressive improvement in self-/cross-correlation suppression. Likewise, examining the right tail of each distribution shows why movers (lying between −100 dB and −85 dB) are obscured for the matched filter, LS-MMF, and MIMO LS-MMF cases. In contrast, MIMO MiCRFt exhibits a "heavy tail" corresponding to the movers since the overall sidelobe response has been significantly reduced.

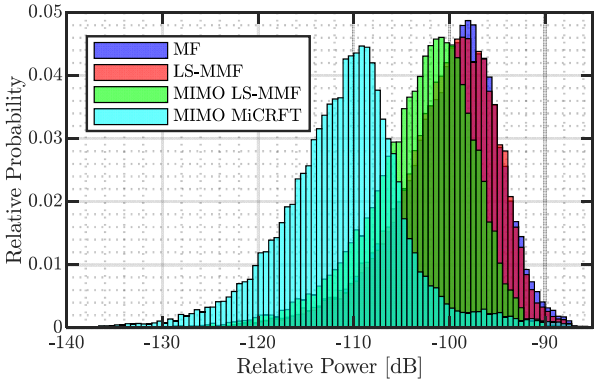

Fig 13: Histograms (in dB) of open-air range-Doppler responses of Figs. 9-12

VII. Conclusions

The mismatched complementary-on-receive filtering (MiCRFt) method from [14, 15] has been extended to account for multiple emitters. Building upon the existing separability provided by the dimensionality of distinct sets of nonrepeating waveforms, this MIMO MiCRFt formulation has been demonstrated via simulation, loopback, and open-air measurements to enable significant improvement in the suppression of both self- and cross-correlation sidelobes. The cost for this improvement is modest mismatch loss and some trade-off in the available Doppler space due to the need for slow-time post-summing.

References

[1] M.C. Wicks, "Sensors as robots," *Intl. Waveform Diversity & Design Conf.*, Lihue, HI, Jan. 2006.

[2] G. Krieger, "MIMO-SAR: opportunities and pitfalls," *IEEE Trans. Geoscience & Remote Sensing*, vol. 52, no. 5, pp. 2628-2645, May 2014.

[3] S.D. Blunt, E.L. Mokole, "An overview of radar waveform diversity," *IEEE Aerospace & Electronic Systems Mag.*, vol. 31, no. 11, pp. 2-42, Nov. 2016.

[4] C. Meng, J. Xu, S. Peng, J. Yang, X. Wang, Y. Peng, "Suppress cross-correlation noise of same frequency coding orthogonal signals in MIMO-SAR," *IET Intl. Radar Conf.*, Xi'an, China, Apr. 2013.

[5] H. Sun, F. Brigui, M. Lesturgie, "Analysis and comparison of MIMO radar waveforms," *Intl. Radar Conf.*, Lille, France, Oct. 2014.

[6] A. Bourdoux, M. Baudin, "PMCW waveform cross-correlation characterization and interference mitigation," *European Radar Conf.*, Utrecht, Netherlands, Jan. 2017.

[7] S.D. Blunt, *et al.*, "Principles and applications of random FM radar waveform design," *IEEE Aerospace & Electronic Systems Mag.*, vol. 35, no. 10, pp. 20-28, Oct. 2020.

[8] S.D. Blunt, K. Gerlach, "Multistatic adaptive pulse compression," *IEEE Trans. Aerospace & Electronic Systems*, vol. 42, no. 3, pp. 891-903, July 2006.

[9] P.M. McCormick, S.D. Blunt, "Shared-spectrum multistatic radar: experimental demonstration using FM waveforms," *IEEE Radar Conf.*, Oklahoma City, OK, Apr. 2018.

[10] M.H. Ackroyd, F. Ghani, "Optimum mismatched filters for sidelobe suppression," *IEEE Trans. Aerospace & Electronic Systems*, vol. AES-9, no. 2, pp. 214-218, Mar. 1973.

[11] D. Henke, P. McCormick, S.D. Blunt, T. Higgins, "Practical aspects of optimal mismatch filtering and adaptive pulse compression for FM waveforms," *IEEE Intl. Radar Conf.*, Washington, DC, May 2015.

[12] J. Jakabosky, S.D. Blunt, B. Himed, "Spectral-shape optimized FM noise radar for pulse agility," *IEEE Radar Conf.*, Philadelphia, PA, May 2016.

[13] M. Coutino, F. Uysal, L. Anitori, "Waveform-aware optimal window function design for mismatched filtering," *IEEE Radar Conf.*, New York City, NY, Mar. 2022.

[14] C.C. Jones, S.D. Blunt, "Mismatched complementary-on-receive filtering of diverse FM waveform subsets," *Intl. Radar Conf.*, Toulon, France, Sept. 2019.

[15] C.C. Jones, C.A. Mohr, P.M. McCormick, S.D. Blunt, "Complementary frequency modulated radar waveforms and optimised receive processing," *IET Radar, Sonar & Navigation*, vol. 15, no. 7, pp. 708-723, Apr. 2021.

[16] M.B. Heintzelman, J.W. Owen, S.D. Blunt, B. Maio, E.D. Steinbach, "Practical considerations for optimal mismatched filtering of nonrepeating waveforms," *IEEE Radar Conf.*, San Antonio, TX, May 2023.

[17] M.J.E. Golay, "Complementary series," *IRE Trans. Information Theory*, vol. IT-7, no. 2, pp. 82-87, Apr. 1961.

[18] C.A. Mohr, P.M. McCormick, S.D. Blunt, "Optimized complementary waveform subsets within an FM noise radar CPI," *IEEE Radar Conf.*, Oklahoma City, OK, Apr. 2018.

[19] C.A. Mohr, S.D. Blunt, "Designing random FM radar waveforms with compact spectrum," *IEEE Intl. Conf. Acoustics, Speech & Signal Processing*, Toronto, Canada, June 2021.